


Spatiotemporal visualization of the terahertz emission during high-power laser-matter interactionA. Gopal,^{1,2,*} A. Woldegeorgis,^{1,2} S. Herzer,¹ and M. Almassarani^{1,2}¹*Institut für Optik und Quantenelektronik, Physikalisch-Astronomische Fakultät,
Friedrich-Schiller-Universität, Max-Wien Platz 1, D-07743 Jena, Germany*²*Helmholtz Institute Jena, Fröbelstieg 3, 07743 Jena, Germany* (Received 21 March 2019; revised manuscript received 13 September 2019; published 25 November 2019)

Single-cycle pulses with multimillion volts per centimeter field strengths and spectra in the terahertz (THz) band have attracted great interest due to their ability to coherently manipulate molecular orientations and electron spins resonantly and nonresonantly. The tremendous progress made in the development of compact and powerful terahertz sources have identified intense laser-thin foil interaction as a potential candidate for high-power broadband terahertz radiation. They are micrometers in size and deliver radially polarized terahertz pulses with millijoule energy and gigawatt peak power. Although several works have been carried out to investigate the terahertz generation process, their origin and angular distribution are still debated. We present here an indisputable study on their spatiotemporal characteristics and elaborate the underlying physical processes via recording the three-dimensional beam profile along with transient dynamics. These results are substructured with the quantitative visualization of the charge particle spectra.

DOI: [10.1103/PhysRevE.100.053203](https://doi.org/10.1103/PhysRevE.100.053203)**I. INTRODUCTION**

Single-cycle pulses with multimillion volts per centimeter field strengths and spectra in the terahertz band have attracted great interest due to their ability to coherently manipulate molecular orientations and electron spins resonantly and nonresonantly [1–4]. Short pulse laser based terahertz sources are compact and economic compared to synchrotrons and free-electron lasers and can routinely deliver terahertz pulses with peak powers above gigawatt level via excitation of DC polarization in organic crystals [5] and through free-electron current generation upon ionizing the media [6–8].

Recent studies have shown that coherent radiation in the terahertz spectral regime can be very efficiently ($\sim 10^{-3}$) excited during the high-power laser-solid interaction [6–17]. However, the most unexpected result comes from the fact that the largest amount of terahertz radiation is generated at the rear surface of the target that is not directly irradiated by the laser pulse [14]. Despite the wider interest and innumerable works carried out in recent years, the origin of the terahertz emission is not yet fully established [6–17]. It is well understood that the incident laser pulse does not propagate through solids beyond the skin depth and also the terahertz radiation generated at the front surface cannot propagate through it, implying that the excitation occurs at the rear surface itself. Hence the electrons generated at the front surface and traveling through the foil and escaping at the rear surface should be responsible for the terahertz emission at the rear surface.

The production of energetic electron, proton, and ion beams from the target rear surface has been a field of intense

study for several decades [18,19]. There are a number of processes through which the laser pulse transfers energy to the particles during the interaction. With the currently available intensities, the laser pulse can provide direct energy transfer only to the electrons mainly via the nonlinear force exerted by the laser pulse, Lorentz force, vacuum heating, etc. [18–21], and they will in turn transfer energy to the positive charges. The energy gained by the electrons varies from keV to several MeVs. For ultrathin targets with thickness comparable to the longitudinal extent of the incident laser pulse, energetic electrons can travel through the target without significant loss and exit at the rear surface and create a strong quasistatic sheath field. The sheath field generated can be comparable to the incident laser field, which in turn ionizes the rear surface and accelerates the positive charges to several MeVs [22]. The escape of the electrons and the subsequent current generation along the target surface to neutralize the charge void, the formation of plasma sheath and acceleration of the sheath charges, etc., all result in the generation of electromagnetic radiation [14,17,23–28]. Although many studies have detailed the optical content of this emission from the target rear surface [25–27], the terahertz band has been simply overlooked. It can be intuitively explained that electromagnetic radiation in the terahertz spectral regime occurs, because the timescale of the particle dynamics lasts several tens of femtoseconds to picoseconds. This notion has led to the first investigation of terahertz generation from the target rear surface [14]. However, the subsequent studies by various groups could not agree on the angular distribution and origin of the terahertz radiation for comparable experimental conditions [7,15–17]. Here we resolve this ambiguity in the understanding of the terahertz radiation generation process and its angular distribution by carrying out a careful study on the three-dimensional (3D) emission pattern of the terahertz radiation and by analyzing its temporal characteristic. Further elaboration is provided with

*amrutha.gopal@uni-jena.de

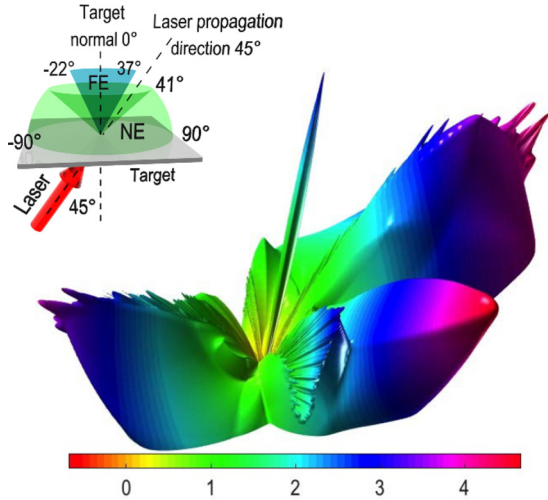


FIG. 1. 3D angular profile of the terahertz radiation emitted from the target rear surface. Inset shows the geometry of the collection angles. FE denotes the emission in the forward direction and NE corresponds to noncollinear direction. Laser pulse is incident onto the thin metal foil target at 45° . Terahertz emission from the rear surface of the target is asymmetric and multiple peaks present in the laser propagation direction. In the Supplemental Material video a 360° perspective of the angular emission can be seen [33].

the electron and proton beam profile emitted from the target rear surface.

II. EXPERIMENT

The experiments were performed at the 40 TW Jena Ti:sapphire laser system (JETI), which delivers 1.2 J, $\lambda_c = 800$ nm, 30 fs pulses at 10 Hz repetition rate. The laser pulses were tightly focused at 45° onto thin ($5 \mu\text{m}$) metal foil targets, leading to intensities $I \geq 10^{19}$ W/cm 2 . The measured temporal contrast of the laser pulse lies in the 10^{-9} – 10^{-7} range in the 5 ps regime and a prepulse of 10^{-4} present at 10 ps before the arrival of the main pulse [29].

Terahertz radiation emitted from the target rear surface was collected in two geometries as shown in the inset of Fig. 1 and the total solid angle of the collection optics was 5.12 sr. Emission in the noncollinear [-90° –($90^\circ \pm 41^\circ$)] direction (NE; light-green shaded area) was collected using an ellipsoidal mirror while in the forward (0 – 22° and $0 + 37.5^\circ$) direction or FE (forward emission; blue shaded area) using an off-axis 3-in.-diameter ($f/1$) parabola. Here 0° corresponds to the target normal direction. The angular distribution of the terahertz emission from the target rear surface was carried out by placing a motorized beam profiler in the collimated beam path and the transmitted energy was recorded with a pyroelectric detector. The beam profiler was translated in vertical and horizontal directions to measure the energy in different regions. The size of the beam profiler (5×5 mm 2) was chosen such that the diffraction effects at long wavelengths are taken into consideration without significantly compromising on spatial resolution. By careful analysis, each section of the collimated beam can be related to certain ϕ and θ on the ellipse. Similarly for the forward emission, also the beam

profile was measured. Finally, the two measurements were combined to obtain the full picture of the terahertz emission from the target rear surface.

The temporal dynamics of the terahertz emission was carried out using a single shot noncollinear electro-optic setup. In this scheme the temporal waveform of the terahertz radiation is mapped directly onto the transversal spatial distribution of the optical probe beam. Towards this end, the beam profiler was removed from the beam path and the pyrodetector was replaced with an electro-optic crystal. About 1% of the main laser energy was coupled out using a leakage mirror to probe the terahertz pulse onto the (110) cut electro-optic crystal. Due to the additional dispersion accumulated on the optical path, the pulse duration of the optical probe was 100 fs. The terahertz and the probe beam enclosed an angle θ at the crystal, so that different spatial regions of the probe see the terahertz electric field at different times and acquire different amounts of ellipticity. The temporal modulation of the polarization was turned into spatial modulation of the intensity by using a prism polarizer as an analyzer and a 16-bit Andor CCD camera. The total observational time window of the setup was defined by the transverse width of the probe and the angle θ between the terahertz beam and the optical probe beam at the crystal, while the temporal resolution was defined by the imaging system. Initial integrated energy measurements using a pyrometer revealed that emission in the forward direction is weaker than in the noncollinear direction. Hence different electro-optic crystals were employed for NE and FE geometries. For measurements in the FE direction a ZnTe (zinc telluride) crystal with thickness $500 \mu\text{m}$ and for NE direction, a GaP (gallium phosphide) crystal with thickness $100 \mu\text{m}$, respectively, were employed [30]. The minimum detectable pulse durations were 250 and 103 fs, respectively, for 500 and $100 \mu\text{m}$ crystal thicknesses. Careful geometrical analysis confirmed that the two regions do not overlap. Further efforts were also made in interpreting the transient signal to avoid saturation effects such as broadening of the peaks.

The proton and ion spectra were measured simultaneously for every shot using a Thomson parabola detector, thus ensuring the same interaction condition for every shot. The spectrometer recorded the proton and ion spectra in the target normal direction with an acceptance angle of $1 \mu\text{sr}$. In order to measure the angular distribution of the particle beams gafchromic film (RCF) [31] stack (for electrons) and CR39 plastic detector [32] for protons and ions were utilized. They were placed at 3.5 and 4.5 cm, respectively, from the focal position in a semicircle configuration behind the target. RCF stack consisted of aluminum filters of variable thickness ranging from $6.5 \mu\text{m}$ to 2 millimeter, thus different layers of the RCF film recorded electrons with different energies. Upon exposure to charge particles the color of the RCF films changed depending on the number density and which were later scanned using an isodensity scanner. On the other hand, CR39 plastic was chemically etched upon exposure to make the particle tracks visible.

III. RESULTS

We begin our discussion with the angular distribution pattern of the terahertz radiation, which has been measured

during high-power laser-thin foil interaction. The results presented in Fig. 1 and the video presented in the Supplemental Material [33] show the 3D beam profile of the terahertz emission from the target rear surface, and it clearly indicates that the emission is asymmetric, contrary to the general notion [15–17]. In fact, multiple peaks are present with variable signal amplitudes suggesting multiple excitation processes. And for a 45° angle of incidence of the excitation laser, the terahertz emission is mostly dominant in the laser propagation direction. Evidently, weak uniform background emission is dominated by strong directional emission closer to the laser propagation direction. Peaked emissions with signal strengths many times higher than the background level clearly indicate the dominance of particle bunches rather than surface currents [23,24,28]. Further nonsymmetric peaks are also visible in the laser propagation direction. If the radiation was generated by the surface currents, a more isotropic emission pattern should have been measured. Importantly, the nonsymmetric emission pattern and weak signal strength near the target surface strengthen the argument that the main contributors could be the charge particle bunches exiting the rear surface. Additionally, the large opening angles of the emission lobes on both sides of the target normal indicate that they are caused by low energy electrons exiting the rear surface or the sheath acceleration process. Further studies were also carried out by measuring the polarization of the radiation. Towards this end, the beam profiler was replaced with a wire-grid polarizer and the results presented in Fig. 2(a) indicate emission is mostly radially polarized, implying charge particle dynamics could be the dominant generation process.

Now the next step would be to understand the temporal structure of the terahertz pulses and thereby the absolute strengths of each emission process. Confirming the beam profile results, multiple pulses with variable amplitudes and durations were present in the time domain for both noncollinear and forward emission geometries. The duration (FWHM) of each pulse is well above the detection bandwidth of the diagnostics defined by the electro-optic function of the crystal (250 and 103 fs, respectively, for forward and noncollinear setups) [30]. In the FE direction three pulses with different field strengths [red line of Fig. 2(b)] are present. These pulses have an average (five shots) temporal width of 356 ± 18 fs, 301 ± 40 fs, and 371 ± 30 fs, respectively. Similarly, the temporal structure of noncollinear emission [green line of Fig. 2(b)] also reveals an initial weaker pulse (~ 1 MV/cm) with an average duration of 331 ± 25 fs followed by a stronger pulse (~ 3 MV/cm) of 308 ± 27 fs duration after 1.49 ps. Another emission with ~ 1.5 MV/cm amplitude and 379 ± 45 fs duration can also be seen after 2.91 ps. Since the pulses are of different amplitudes and the separation between them does not match the extra distance the pulse might have encountered due to any kind of internal reflections in the beam path, we can rule out the possibility of the three pulses being the same. Importantly the separation between the pulses and the FWHM are comparable for both NE and FE measurements irrespective of different collection optics and beam relay system employed, a strong indication that there are three distinct generation processes. In order to understand the disparity in the strength of the pulses observed in the two directions, it is necessary to take into consideration the emission angles of

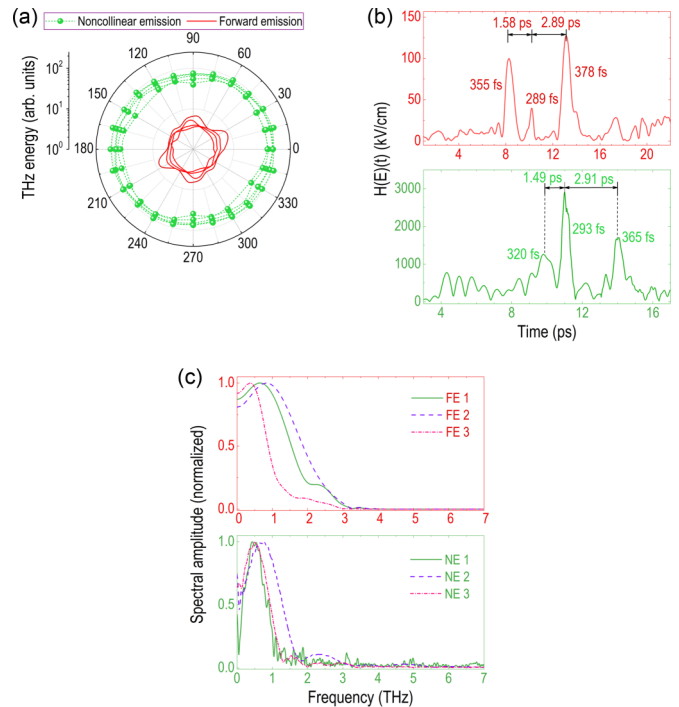


FIG. 2. (a) The polarization of the terahertz radiation measured using a wire-grid polarizer. (b) Transient structure of the terahertz radiation obtained from the electro-optic (EO) measurement for a single shot. Noncollinear (NE) or wide-angle emission (light-green area of Fig. 1 inset) and forward emission (FE; blue area marked in Fig. 1 inset) using balanced detection scheme. Multiple pulses are present both in the wide-angle and forward emission with similar pulse durations and comparable temporal delays. (c) Spectral intensity of the terahertz pulses.

physical process and the collection angles of the respective measurement setups. The discrepancy in the signal amplitude emerging from the collection optics can be estimated if the terahertz emission is uniform. As one sees from the beam profile, the terahertz emission is stronger along the laser propagation direction and the noncollinear setup collects more radiation than the forward setup. The above arguments suggest that multiple pulses in the temporal domain and multiple peaks in the beam profile are due to different generation processes. Moreover, the EO measurements confirm that the terahertz radiation is coherent and the integrated signal from the EO detection scheme matches with the corresponding value obtained from the beam profile measurements. Hence it is obvious to assume that the emission can only be caused by the charge particle dynamics at the target rear surface. The fact that all the pulses have a FWHM duration above the temporal resolution of the diagnostic, suggests that the measurements are the actual transient duration of the charge particle dynamics at the rear surface, which is the genesis of coherent terahertz emission. Furthermore, the spectral content of the pulses presented in Fig. 2(c) obtained from the Fourier transform of the temporal measurements [Fig. 2(b)] did not show significant differences except for the second peak, which is slightly blueshifted and the central frequencies were gathered around 1 THz. The blueshift of the spectra of peak 2 in

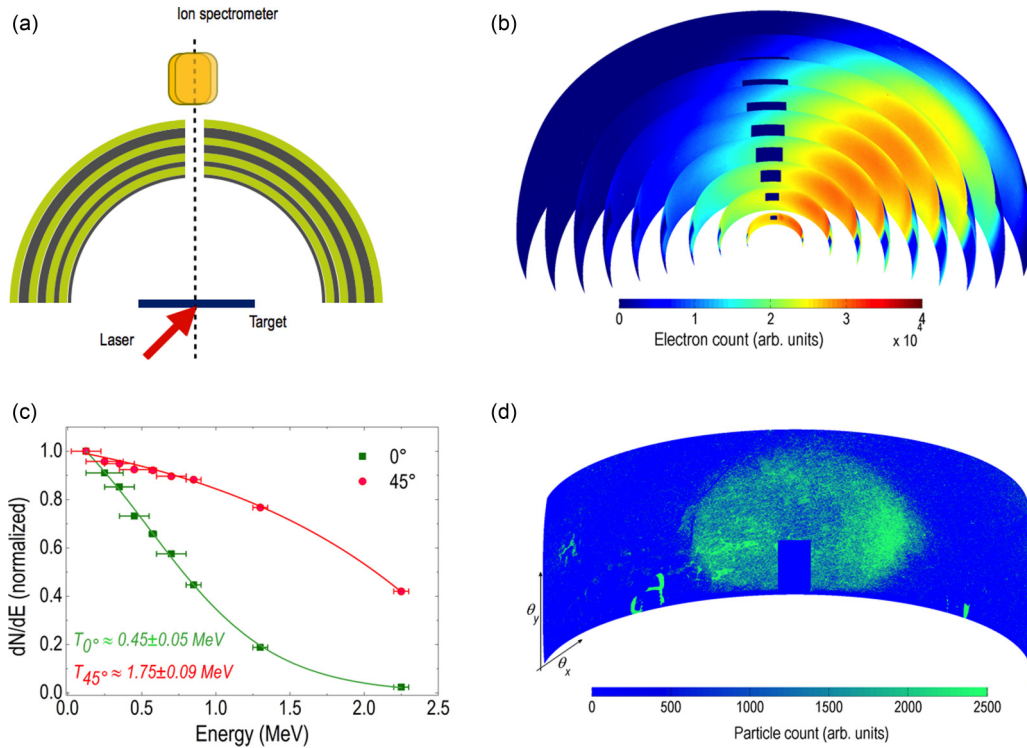


FIG. 3. (a) Schematic of the particle detection scheme. (b) Angular distribution of the electron beam detected using gafchromic films with different thickness aluminum filters. The hole represents the target normal direction. Clearly, low energy background emission is dominated by energetic electrons emitted in the laser propagation direction. (c) Energy spectra of the electrons measured along 0° (target normal) and 45° (laser propagation direction). (d) Proton and ion beam angular distribution recorded by the CR39 plastic detector.

both measurements may suggest Doppler shifting due to the energetic charge or particle motion.

In order to shine further light on the origin of the physical processes, let us dissect the beam profile into several sections. For a 45° angle of incidence the emission is dominant and strong on both sides of laser propagation direction ($\theta = 45 \pm 21^\circ$). The features of this emission are closer to transition radiation by energetic electrons pushed in the laser propagation direction by the laser ponderomotive force. The narrow peak close to the laser propagation direction is about $23 \pm 2^\circ$ corresponding to a peak electron energy of 2.25 MeV. In Fig. 1, the left lobe of this emission can be seen between target normal (TN) and laser propagation direction. The other lobe is immersed in the emission close to the target surface where wide-angle contribution dominates. Indeed it has also been confirmed experimentally that for similar laser intensities, the fast electron current generated by the ponderomotive heating has similar energies [29,34,35]. Furthermore, a clear dipolelike emission close to the target surface is also visible with close to symmetric distributions, suggesting the emission driven by very low energy electrons with temperatures 0.45 MeV or by the expansion of the plasma sheath at the target rear surface.

To elaborate further the above arguments, let us look at the recorded electron [Fig. 3(b)] and proton beam profiles [Fig. 3(d)] behind the target during the terahertz generation process using gafchromic film stacks and CR39 plastic detectors, respectively. As seen in Fig. 3(b), the front layer exhibits uniform distribution of low energy electrons (30–125 keV) behind the target. As the thickness of the aluminum filter

increases, this uniform distribution shrinks and the energetic electrons concentrate more towards the laser propagation direction. In the target normal direction, where sheath acceleration takes place, the maximum energy of the electrons is < 850 keV, agreeing with previous observations. On the other hand, the electron beam in the laser propagation direction has peak energies extending above 2.25 MeV.

Unlike the electron beam, the proton beam profile behind the target is more localized in the target normal direction with a half angle divergence of 23° . The maximum proton energy measured in the target normal direction using an ion spectrometer exceeded 3.7 MeV. Like previously mentioned, the electron beam profile indicates that there are various processes through which the electrons gain energy from the incident laser pulse. In fact, the peak energies and angular distribution of the electrons generated from different processes vary. For instance, the ponderomotively heated electrons are pushed in the laser propagation direction, while the electrons which gain energy due to resonance absorption or Brunel heating will exit mainly in the target normal direction with lower peak energies [20,34–38]. The electron spectra presented in Fig. 3(c) confirm that the temperatures of the electrons exiting in the two directions are different [20,37]. The temperatures of the two beams are 0.45 ± 0.05 MeV and 1.75 ± 0.09 MeV in the TN and laser propagation (LP) directions and they agree with the established scaling laws [39].

The availability of both electron and proton beam angular distribution and spectra enabled us to estimate the coherent transition radiation generated by the electrons exiting the target rear surface in the TN and LP directions and radiation

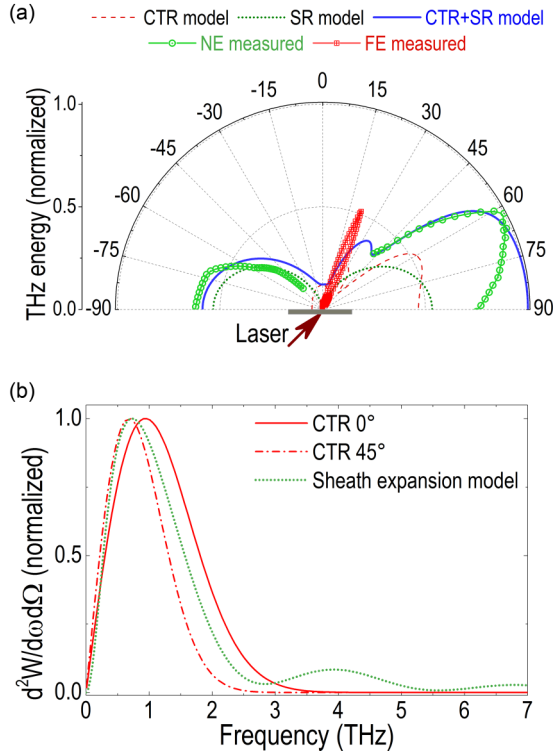


FIG. 4. (a) Angular intensity distributions of coherent transition radiation (CTR) emission estimated for the electrons exiting the target rear surface (red line) and sheath radiation emitted by the plasma expansion (green line). Solid blue line is the sum of the CTR and sheath radiation emission estimated numerically. Red squares and green circles represent the experimental data taken from Fig. 1. (b) The corresponding spectral distributions of the radiation calculated from the electron distribution taken from Fig. 3(c). CTR 0°, solid red line; CTR 45°, dotted red line; and solid green line, the sheath radiation emitted by the expanding plasma sheath formed in the target normal direction at the rear surface.

emitted by the expansion of the plasma sheath during the ion acceleration process [40–47]. For the estimation of the coherent sheath radiation the electron and proton or ion spectra recorded in the target normal direction was employed. Here we assumed the plasma sheath to be a transient electric dipole that comprises the electron population at the plasma front and the ions following them. The proton and ion beam profile allowed us to estimate the sheath size behind the target. This calculation was compared with the projection of laser focal spot on the target rear surface.

Figure 4(a) (red line) presents the estimated angular distribution of the combined coherent transition radiation emitted by the electron spectra shown in Fig. 3(c) exiting the target rear surface and the green line presents the sheath radiation from the sheath acceleration process generating the proton spectra shown in Fig. 3(d). The sum of three emissions estimated numerically is presented by a solid blue line. Red squares and green circles represent the experimental data taken from Fig. 1. Very good agreement between the experimentally measured terahertz radiation (Fig. 1) and the calculated terahertz beam profile [Fig. 4(a)] comply with our argument of the terahertz generation process driven by charge particle dynamics at the target rear surface. The corresponding

spectra of the coherent transition radiation (CTR) emissions are given in Fig. 4(b) (red lines), which show spectral components extending up to 2.4 THz for electrons escaping at 45° and 1.7 THz for electrons exiting in the target normal direction. This difference in the spectral width implies different temporal duration measured for the corresponding terahertz pulses. The spectra of the coherent sheath radiation is presented in Fig. 4(b) (green line). Similar to the experimentally recorded spectra [Fig. 2(c)] the results from the numerical estimates indicate different spectral bandwidth related to the emission process.

IV. DISCUSSION AND SUMMARY

Given the good agreement between the experimentally measured and calculated terahertz beam profile and spectra, we may now compare the contribution due to various effects on coherent terahertz generation from the target rear surface. Here one needs to bear in mind that electromagnetic radiation in the terahertz and lower frequencies could also be generated at the bulk target due to electrons moving along the surface [23,24,28,36,48]. However, in our measurements this contribution is insignificant as the terahertz beam profile presented in Fig. 1 does not show significant emission close to the target surface. Similarly the integrated signal strength obtained from the beam profile and EO diagnostic were comparable suggesting that the contribution of incoherent radiation in the beam profile is negligible. Considering the time taken by the charged particles to traverse the target and looking at the geometry of the emission and amplitude of the transient peaks, we can attribute the first peak observed in both measurements to be the CTR emission due to the electrons escaping in the target normal direction. The strong second peak in NE and weak second peak in FE arise from the CTR process driven by the energetic electrons pushed by the ponderomotive force of the laser exiting in the target rear surface. In fact, this is the strongest emission seen in the beam profile but also contains high frequency components extending beyond optical regime [10]. The temporal durations from both measurements are comparable while disparity in the field strengths can be attributed to the solid angles of the collection optics. Indeed, the collection optics employed for the FE measurements did not gather the whole left lobe of this CTR emission. Moving on further, the third pulse present after 2.89 ± 0.02 ps can be attributed to the sheath acceleration process. This dipolelike emission is driven by the low energy electrons exiting in the target normal direction and subsequently generating the plasma sheath and accelerating the positive charges. Even though these electrons are less energetic compared to the ones exiting at 45°, their number density is high enough to accelerate $\sim 10^9$ protons. This emission is also wide angle so mostly collected by the NE, hence the amplitude of this emission is higher in the NE measurements than FE. Although the sheath acceleration process occurs about 4.47 ± 0.04 ps after the electrons exit the target rear surface, the timescale of the acceleration process is 379 ± 35 fs. This implies that positive charges gain most of the energy in this timescale as no further weaker pulses were present in either of the measurements.

Compared to previous works, here we identify the presence of three distinct peaks in the EO optic measurements, suggesting that there are three processes responsible for coherent terahertz generation from the target rear surface. The emission processes clearly depend on the electron distribution at the rear of the target which in turn are influenced by the incident laser parameters and temporal contrast. Here we point out that the absence of multiple pulses from previous studies can be attributed to the EO detection scheme and the solid angle of the collection optics. For instance, the EO signals generated by different processes have different amplitudes, thus requiring careful filtering to obtain all the emissions in a single observation window without saturation effects.

We have presented a distinct picture of the terahertz emission from the rear surface of a thin metal foil when it is shined with a multiterawatt laser pulse at oblique incidence. The 3D angular plot suggests that the terahertz emission is more dominant at large angles with respect to the target normal direction for oblique incidence of the incident laser agreeing with the calculations using experimentally measured charged particle spectra. The temporal structures present short, multiple pulses of few hundreds of femtosecond duration lasting for several picoseconds, which points towards at least two telltale emission processes such as coherent transition radiation and sheath radiation. For ultra short-pulse (<100 fs) laser-solid interaction at oblique angle of incidence with intensities reaching up to several 10^{19} W/cm², electron beams with different

temperatures can be generated, which in turn will emit CTR in the terahertz range. The angular distribution and the temporal duration of these emissions are dependent on the electron temperature which is influenced by the temporal contrast and polarization of the incident laser along with incident angle and target parameters [18,19,34,35,37,38,49]. The intriguing fact that the electron exiting in the LP direction takes ~ 1.5 ps additional time than the one exiting in the TN direction requires further investigation using different target thickness, simulations, etc. As mentioned before, depending on the interaction conditions the dominant electron heating mechanisms will change thereby influencing the angular distribution of the terahertz emission. Hence it would be worthwhile to investigate the influence of those parameters on the rear surface terahertz emission along with the angular spectra of the particle to gain further insight into the complex dynamics of laser matter interaction. In other respects the possibility to generate multiple terahertz pulses with MV/cm electric field strengths provides unique opportunities in terahertz pump-probe studies.

ACKNOWLEDGMENTS

This work is supported by the Deutsche Forschungsgemeinschaft through Grant No. Go 1998/3-1. The authors also thank F. Ronneberger, B. Beleites, R. Grosse, T. May, and A. Brömmel for the technical support during the experimental campaigns.

-
- [1] C. Vicario, B. Monoszalai, and C. P. Hauri, *Phys. Rev. Lett.* **112**, 213901 (2014).
 - [2] D. Nicoletti and A. Cavalleri, *Adv. Opt. Photonics* **8**, 401 (2016).
 - [3] J. Walkowski and M. Münzenberg, *J. Appl. Phys.* **120**, 140901 (2016).
 - [4] S. Wienholdt, D. Hinzke, and U. Nowak, *Phys. Rev. Lett.* **108**, 247207 (2012).
 - [5] M. Shalaby, C. Vicario, and C. P. Hauri, *APL Photonics* **2**, 036106 (2017).
 - [6] H. Hamster, A. Sullivan, S. Gordon, W. White, and R. W. Falcone, *Phys. Rev. Lett.* **71**, 2725 (1993).
 - [7] A. Gopal *et al.*, *Phys. Rev. Lett.* **111**, 074802 (2013).
 - [8] A. Woldegeorgis *et al.*, *Optica* **5**, 1474 (2018).
 - [9] A. Gopal *et al.*, *Opt. Lett.* **38**, 4705 (2013).
 - [10] S. Herzer *et al.*, *New J. Phys.* **20**, 063019 (2018).
 - [11] A. Sagisaka *et al.*, *Appl. Phys. B* **90**, 373 (2008).
 - [12] C. Li, M. L. Zhou, W. J. Ding, F. Du, F. Liu, Y. T. Li, W. M. Wang, Z. M. Sheng, J. L. Ma, L. M. Chen *et al.*, *Phys. Rev. E* **84**, 036405 (2011).
 - [13] Y. T. Li *et al.*, *Appl. Phys. Lett.* **100**, 254101 (2012).
 - [14] A. Gopal *et al.*, *New J. Phys.* **14**, 083012 (2012).
 - [15] G. Q. Liao, Y. Li, H. Liu, G. G. Scott, D. Neely, Y. Zhang, B. Zhu, Z. Zhang, C. Armstrong, E. Zemaityte *et al.*, *Proc. Natl. Acad. Sci. USA* **116**, 3994 (2019).
 - [16] Z. Jin *et al.*, *Phys. Rev. E* **94**, 033206 (2016).
 - [17] G. Q. Liao, Y. T. Li, Y. H. Zhang, H. Liu, X. L. Ge, S. Yang, W. Q. Wei, X. H. Yuan, Y. Q. Deng, B. J. Zhu *et al.*, *Phys. Rev. Lett.* **116**, 205003 (2016).
 - [18] H. Daido *et al.*, *Rep. Prog. Phys.* **75**, 056401 (2012).
 - [19] A. Macchi, M. Borghesi, and M. Passoni, *Rev. Mod. Phys.* **85**, 751 (2013).
 - [20] P. Gibbon, *Short Pulse Laser Interactions with Matter* (Imperial College Press, London, 2005).
 - [21] W. L. Kruer *et al.*, *Phys. Fluids* **28**, 430 (1985).
 - [22] S. C. Wilks *et al.*, *Phys. Plasmas* **8**, 542 (2001).
 - [23] A. Poyé *et al.*, *Phys. Rev. E* **91**, 043106 (2015).
 - [24] M. J. Mead *et al.*, *Rev. Sci. Instrum.* **75**, 4225 (2004).
 - [25] J. J. Santos *et al.*, *Phys. Rev. Lett.* **89**, 025001 (2002).
 - [26] S. D. Baton *et al.*, *Phys. Rev. Lett.* **91**, 105001 (2003).
 - [27] C. Bellei *et al.*, *New J. Phys.* **12**, 073016 (2010).
 - [28] C. G. Brown, Jr. *et al.*, *J. Phys. Conf. Ser.* **112**, 032025 (2008).
 - [29] A. H. Woldegeorgis, B. Beleites, F. Ronneberger, R. Grosse, and A. Gopal, *Phys. Rev. E* **98**, 061201(R) (2018).
 - [30] S. Casalbuoni, B. Schmidt, P. Schmäser, V. Arsov, and S. Wesch, *Phys. Rev. ST. Accel. Beams* **12**, 030705 (2009).
 - [31] S. Devic, *Phys. Medica* **27**, 122 (2011).
 - [32] H. A. Khan *et al.*, *Nucl. Tracks Radiat. Meas.* **7**, 129 (1983).
 - [33] See Supplemental Material at <http://link.aps.org/supplemental/10.1103/PhysRevE.100.053203> for a video showing the 360° perspective of the angular emission of terahertz radiation.
 - [34] Y. Ping *et al.*, *Phys. Rev. Lett.* **100**, 085004 (2008).
 - [35] P. K. Singh *et al.*, *Sci. Rep.* **5**, 17870 (2015).
 - [36] H. B. Zhuo *et al.*, *Phys. Rev. E* **95**, 013201 (2017).
 - [37] B. I. Cho, J. Osterholz, A. C. Bernstein, G. M. Dyer, A. Karmakar, A. Pukhov, and T. Ditmire, *Phys. Rev. E* **80**, 055402(R) (2009).
 - [38] H. Liu *et al.*, *Rev. Sci. Instrum.* **89**, 083302 (2018).

- [39] W. L. Kruer, *Physics of Laser Plasma Interactions* (Addison-Wesley, Menlo Park, CA, 1988).
- [40] J. D. Jackson, *Classical Electrodynamics*, 3rd edition (Wiley, New York, 1999), Chap. 14.
- [41] V. L. Ginzburg and V. N. Tsytovich, *Transition Radiation and Transition Scattering* (Adam Hilger, New York, 1990).
- [42] W. P. Leemans *et al.*, [Phys. Rev. Lett. **91**, 074802 \(2003\)](#).
- [43] J. van Tilborg *et al.*, [Laser Part. Beams **22**, 415 \(2004\)](#).
- [44] W. P. Leemans *et al.*, [Phys. Plasmas **11**, 2899 \(2004\)](#).
- [45] C. B. Schroeder, E. Esarey, J. van Tilborg and W. P. Leemans, [Phys. Rev. E **69**, 016501 \(2004\)](#).
- [46] J. van Tilborg *et al.*, [Phys. Rev. Lett. **96**, 014801 \(2006\)](#).
- [47] A. Woldegeorgis *et al.*, [Phys. Rev. E **100**, 053204 \(2019\)](#).
- [48] Y. Gao *et al.*, [Opt. Lett. **33**, 2776 \(2008\)](#).
- [49] F. N. Beg *et al.*, [Phys. Plasmas **4**, 447 \(1997\)](#).